The Linnean Society of London
ZOOLOGICAL Journal of the Linnean Society

Two parasitic ciliates (Protozoa: Ciliophora: Phyllopharyngea) isolated from respiratory-mucus of an unhealthy beluga whale: characterization, phylogeny, and an assessment of morphological adaptations

Journal:	*Zoological Journal of the Linnean Society*
Manuscript ID	ZOJ-03-2020-4042.R1
Manuscript Type:	Original Article
Keywords:	morphology < Anatomy, new species < Taxonomy, phylogeny < Phylogenetics, ultrastructure < Anatomy
Abstract:	Ciliates occur in the blowholes of marine mammals, but our understanding of their biology is poor. Consequently, we investigated an infestation of ciliates in an unhealthy, captive beluga whale that was exhibiting accelerated breathing, leukocytosis, and expulsion of unusually large amounts of viscous sputum. This sputum contained ~104 ciliates per ml-1 (when healthy, numbers were 10- to 100-fold lower). One known ciliate species, Planilamina ovata Ma et al., 2006, was fully characterized, and a new species, Kyaroikeus paracetarius sp. nov., was described. The new species is established based on its lager number of left kineties over its only congener. Moreover, new sequences of small-subunit rDNA, large-subunit rDNA, and ITS1-5.8S-ITS2 regions of these two taxa provided phylogenetic analyses; these inferred that Kyaroikeus and Planilamina have close affinity with the free-living family Dysteriidae, contradicting their morphology-based assignment to the family Kyaroikeidae (we suggest the Kyaroikeidae be relegated to sub-family status). Finally, by comparing the parasitic species with free-living taxa, we suggest how these ciliates have adapted to their unique environment and how they may have initially invaded the host. In short, we provide essential data and concepts for the continued evaluation of ciliate-parasites in beluga whale blowholes.

SCHOLARONE™
Manuscripts

ABSTRACT

Ciliates occur in the blowholes of marine mammals, but our understanding of their biology is poor. Consequently, we investigated an infestation of ciliates in an unhealthy, captive beluga whale that was exhibiting accelerated breathing, leukocytosis, and expulsion of unusually large amounts of viscous sputum. This sputum contained ~10^4 ciliates per ml^{-1} (when healthy, numbers were 10- to 100-fold lower). One known ciliate species, *Planilamina ovata* Ma *et al*., 2006, was fully characterized, and a new species, *Kyaroikeus paracetarius* sp. nov., was described. The new species is established based on its lager number of left kineties over its only congener. Moreover, new sequences of small-subunit rDNA, large-subunit rDNA, and ITS1-5.8S-ITS2 regions of these two taxa provided phylogenetic analyses; these inferred that *Kyaroikeus* and *Planilamina* have close affinity with the free-living family Dysteriidae, contradicting their morphology-based assignment to the family Kyaroikeidae (we suggest the Kyaroikeidae be relegated to sub-family status). Finally, by comparing the parasitic species with free-living taxa, we suggest how these ciliates have adapted to their unique environment and how they may have initially invaded the host. In short, we provide essential data and concepts for the continued evaluation of ciliate-parasites in beluga whale blowholes.

KEYWORDS: *Kyaroikeus paracetarius* sp. nov. – morphology – multi-gene sequences – new species – phylogeny – ultrastructure.

For Review Only

INTRODUCTION

The phylum Ciliophora is ubiquitous and diverse, with on the order of 10,000 species comprising free-living, commensal, and parasitic forms (Hu *et al*., 2019; Lynn, 2008; Song *et al*., 2009). Although, a large number of ciliates are parasites of aquatic invertebrate and fish, few seem to parasitize aquatic mammals. Of note are the blood-feeding prostomatean ciliate *Haematophagus megapterae* that infects the baleen plates of humpback, fin, and blue whales and the litostomatean ciliates *Balantidium* spp., found in the large intestine and feces of sea lions and fin whales (Hermosilla *et al*., 2015, 2016). Some uncharacterized ciliates are also associated with the skin, blowholes, air sacs, bronchiole, lungs, lymph node, and faeces of dolphins and whales (Lair *et al*., 2016; McFee & Lipscomb, 2009; Poynton *et al*., 2001).

All of the ciliates associated with marine mammals are thought to elicit low pathogenicity or at least act as opportunists, invading ulcerated areas, especially in cetaceans in unhealthy condition (Choi *et al*., 2003; Gulland *et al*., 2018). To appreciate the impact of ciliates on the health of cetaceans there is, therefore, a need to both report cases of such instances and, critically, identify the invasive taxa. To this end we report on the abundance, morphology, phylogenetic position, and adaptive traits of one known and one new ciliate species, found at unprecedented abundances in the respiratory tract of a beluga whale that was suffering from respiratory problems.

MATERIALS AND METHODS

SAMPLE COLLECTION

Samples were collected from a solitary ~10-year-old beluga whale (*Delphinapterus leucas*), kept in captivity for ~6 years in Ningbo Aquarium, China (Supplementary Figure S1, picture of the white beluga). This intensely managed aquarium is a closed system, with all water (~18.0 °C, ~28 PSU, pH 7.8, total nitrogen 0.05 mg L^{-1}, nitrite 0.05 mg L^{-1}) recirculated and periodically sterilized. The beluga whale was contained in a 2500 m^3 (about 400 m^2, average water depth 5 m) enclosure. It was fed four times a day, most with wild caught herring and capelin, with a total amount of about 18 kg per day.

In May 2017 the beluga whale exhibited abnormal behavior, frequently floating on the water or lying sideways, sometimes standing upright by the side of the pool, and rubbing the wall with the outer margin of its blowhole. Its breathing frequency increased to 4 min^{-1} (normally 1 to 3 min^{-1}), and it often exhaled aggressively to expel mucus, which contained exfoliated epithelial tissue. Moreover, blood test indicated leukocytosis (conducted by the facility's veterinarian, Supplementary Data S1, blood test index of beluga whale), a clear sign of poor health (Norman *et al*., 2012). Expelled mucus (including epithelial tissue) was obtained using two methods: 1) when the amount of released mucus with epithelial tissue was large, the floating mucus was collected directly into a container; 2) when floating mucus was not available, nasal mucus was collected from the host directly; the beluga whale was encouraged to rest its head on the pool bank, and after ~5 exhalations, the veterinarian collected the mucus

For Review Only

(Supplementary Figure S1C, Ma *et al*., 2006). The mucus with epithelial tissue was directly examined using a stereomicroscope; ciliates were collected using a micropipette and observed by compound microscopy. Abundance was determined by placing 50 μl of mucus, containing flocs of epithelial tissue, on a microscope slide and counting cells. About 200 individuals were isolated and examined following the recommendations of Warren *et al*. (2017), as outlined below. The movement and feeding of the new species were recorded (Supplementary Video S1, filming of movement and feeding). In December 2019 the beluga whale had fully recovered and was in a healthy state (i.e. no abnormal behavior, blood tests indicated good health, no mucus expelled in the water, very little exfoliated epithelial tissue in the mucus; Supplementary Figure S2); at this time to assess for abundance of ciliates the mucus was collected directly from the blowhole four times, one week apart.

OPTICAL MICROSCOPY AND IDENTIFICATION

Immediately after collecting mucus, the live morphology of the ciliates was studied using a compound microscope equipped with differential interference contrast. The ciliary pattern and nuclear apparatus were revealed by protargol staining (Wilbert, 1975), using protargol synthesized following the protocol of Pan *et al*. (2013). Morphometric measurements were conducted at a magnification of 1000 ×. Illustrations of the stained specimens were made with the aid of a camera lucida. Terminology followed Ma *et al*. (2006), Lynn (2008), and Chen *et al*. (2016).

SCANNING AND TRANSMISSION ELECTRON MICROSCOPY (SEM AND TEM)

SEM and TEM studies were only conducted on *Kyaroikeus paracetarius* sp. nov., as preparations for *Planilamina ovata* Ma *et al*., 2006 failed. The procedures of SEM mainly follow Ma *et al*. (2016). Cells were fixed in 2.5 % glutaraldehyde and stored at 4 °C. Subsequently, cells were washed three times in 0.1 M phosphate buffer (pH 7.0) to remove fixative. After alcohol dehydrations and critical point drying by CO_2 (Leica EM CPD300), cells were coated with platinum in Leica EMACE600. Observations were made using a Hitachi S-4800 scanning electron microscope with accelerating voltage of 3.0–5.0 kV.

TEM preparation also follows Ma *et al*. (2016). 2.5 % glutaraldehyde fixed cells were washed and post-fixed in 1 % phosphate buffered OsO_4 for 1 h at 4 °C. After three washes in the cacodylate buffer, specimens were processed through alcohol dehydrations and acetone dehydrations. Then cells were embedded in Epon 12 and polymerized at 37 °C for 16 h, 45 °C for 24 h, and 60 °C for 48 h. Thin sections were placed on copper grids using uranyl acetate and lead citrate for staining. These were observed under a Hitachi HT7700 transmission electron microscope with accelerating voltage of 100 kV.

DNA EXTRACTION, PCR AND MULTI-GENE SEQUENCING

Clonal cultures could not be established. Instead, for each species, cells were collected, optically

For Review Only

identified, and then single cells were isolated. These cells were washed four times in filtered habitat water (0.22 µm-pore size membrane, Millipore, USA), washed two times in ultra-pure water, and then placed in 1.5 ml microfuge tubes with ~45 µL of buffer. For both species this process was repeated on three dates (2 May, 2017; 4 June, 2017; 1 January, 2018), providing sequence data for the equivalent of three clonal isolates per species. Genomic DNA was extracted following the manufacturer's instructions (Dneasy Blood and Tissue Kit, Qiagen, Hilden, Germany). The small-subunit (SSU) rDNA was amplified with the universal eukaryotic primers 18SF (5′-AAC CTG GTT GAT CCT GCC AGT-3′) and 18SR (5′-TGA TCC TTC TGC AGG TTC ACC TAC-3′) (Medlin *et al*., 1988). A fragment of ~500 bp containing the internal transcribed spacer regions 1 and 2 (ITS-1, ITS-2) and 5.8S ribosomal gene was amplified using primers 5.8SF (5′-GTA GGT GAA CCT GCG GAA GGA TC-3′) and 5.8SR (5′-CTG ATA TGC TTA AGT TCA GCG G-3′) (Yi *et al*., 2009). The large-subunit (LSU) rDNA was amplified using the primers 28S-F3 (5′-TAC TGA TAT GCT TAA GTT CAG CGG-3′) and 28S-R2 (5′-AAC CTT GGA GAC CTG AT-3′) (Moreira *et al*., 2007).

PCR conditions for the three DNA segments were the same and were as follows: 1) initial denaturation for 30 s at 98 °C; 2) 35 cycles of 10 s denaturation at 98 °C, 20 s primer annealing at 56 °C, and 100 s primer elongation at 72 °C; and 3) final primer elongation for 120 s at 72 °C. Q5 Hot Start High-Fidelity DNA Polymerase (NEB Co, Ltd, M0493, Beijing) was used to minimize the possibility of PCR amplification errors. Purifying of PCR products, cloning and sequencing were performed (Wang *et al*., 2017).

PHYLOGENETIC ANALYSES

Six new sequences (SSU rDNA, ITS1-5.8S-ITS2 region, and LSU rDNA) of *Kyaroikeus paracetarius* sp. nov. and *Planilamina ovata* were sequenced and are provided here. Other sequences used in our phylogenetic analyses were obtained from NCBI GenBank database, including: 1) SSU rDNA sequences of 35 dysteriids, 41 chlamydodontids, and 6 suctorians; 2) ITS1-5.8S-ITS2 region sequences of 1 dysteriid, 5 chlamydodontids, and 2 suctorians; 3) LSU rDNA sequences of 1 dysteriid, 3 chlamydodontids, and 2 suctorians. The suctorians mentioned above were used as out-group taxa, because subclass Suctoria is phylogenetically close to subclass Cyrtophoria.

Sequences were aligned using Clustal W implemented in Bioedit v7.1.3.0 using the default parameters (Hall, 1999). The resulting alignments were manually refined by trimming both ends. Maximum likelihood (ML) analyses were conducted on CIPRES Science Gateway with RAxML-HPC2 on XSEDE v8.2.4 (Stamatakis *et al*., 2008) using the GTR + I + G model as optical according to the AIC criterion by Modeltest v3.4 (Posada & Crandall, 1998). Support for the best ML tree was from 1000 bootstrap replicates. A Bayesian inference (BI) analysis was performed on CIPRES Science Gateway with MrBayes on XSEDE v3.2.6 (Ronquist & Huelsenbeck, 2003) using the GTR + I + G model (selected by MrModeltest v2.2) (Nylander, 2004). The chain length of Markov chain Monte Carlo simulations was 10^6 generations with a sampling frequency of every 100th generation. The first

For Review Only

25 % of the sampled trees was discarded as burn-in. Phylogenetic trees were visualized via MEGA v5.0 (Tamura *et al*., 2011) and TreeView v.1.6.6 (Page, 1996). Systematic classification mainly followed Lynn (2008), Gao *et al*. (2016), and Chen *et al*. (2016).

RESULTS

Two ciliate species were abundant in the mucus of the unhealthy beluga whale: *Kyaroikeus paracetarius* sp. nov. (~ 2.5×10^4 ml^{-1}) and *Planilamina ovata* Ma *et al*., 2006 (~ 5.0×10^3 ml^{-1}). These ciliates were also found in the mucus when the beluga whale was healthy, but at much lower numbers: *K. paracetarius* (~ 2×10^3 ml^{-1}), *P. ovata* was very rare (< 1×10^2 ml^{-1}) or absent. The ciliates always attached to the surface of the flocs of exfoliated epithelial tissue and fed on the epithelial cells.

All isolated ciliates died within 24 h of leaving the host, regardless of being maintained at 18 ºC (water temperature), 25 ºC (air temperature), or 35 ºC (host body temperature) in mucus samples or mucus diluted to different salinities (0, 5, 10, 15, 20, 28 PSU) (Supplementary Data S2, cultivation data of the new species). We were, therefore, not able to culture either taxa. However, it was possible to isolate individuals of both taxa, identify *P. ovata* (provide a re-description of it), and provide a formal, detailed description of the new species. To this end, three isolations of *Kyaroikeus paracetarius* sp. nov. and three isolates of *Planilamina ovata* were made on different dates (see Methods); DNA sequences isolated from replicate clones were identical, and the two species were distinct.

ORDER DYSTERIIDA DEROUX, 1976

FAMILY KYAROIKEIDAE SNIEZEK & COATS, 1996

GENUS KYAROIKEUS SNIEZEK ET AL., 1995

KYAROIKEUS PARACETARIUS SP. NOV. (Figs 1–5; Table 1)

Diagnosis. Size 150–400 × 20–40 μm *in vivo*; spindle-shape; deep oral cavity composed of a preoral kinety and two circumoral kineties; no nematodesmal rods; 37–69 right kineties, 7–13 left kineties; four kinetofragments located near equatorial position; equatorial fragment positioned next to the middle part of the rightmost right kinety; non-ciliated stripe underlain by 11–16 fibrous tracks; a bifurcated secretory organelle opened at the tip of podite; one ovoid macronucleus.

Host. *Delphinapterus leucas* Pallas, 1776 (beluga whale).

Etymology. The species name *paracetarius* is a composite of the Greek prefix *para-* (beside) and the species-group name *cetarius*, indicating that the new species is morphologically similar to *Kyaroikeus cetarius*.

For Review Only

Type material. One slide with a protargol-stained holotype specimen (indicated with a black circle of ink on the coverslip) and several paratype specimens has been deposited in the Laboratory of Protistology, Ocean University of China (OUC) with registration number LJ-I-20170502-01. Two slides with protargol-stained paratype specimens were deposited in the collection of Ningbo University (registration numbers: LJ-I-20170502-02, LJ-I-20170502-03).

ZooBank accession number of the new species. urn:lsid:zoobank.org:act:199C1DAD-F159-4EA7-ACB2-C03492F12B00

General morphology and ciliary pattern. Body size 150–400 × 20–40 μm *in vivo* and 150–365 × 35–80 μm after protargol staining. Long spindle-shaped body with a length-width ratio of ~10:1, neither bilateral nor dorso-ventral compressed (Figs 1A, B, 2A, 3A). Pellicular ridges distributed on surface of cell, between adjacent somatic kineties; densely packed kinetosomes located at base of these ridges (Fig. 3H, I). Conspicuous bipolar, non-ciliated stripe located on left ventral surface, 10–30 μm wide (Figs 1C, D, H, 2F, R, 3B–F). Eleven to 16 pellicular folds situated on "naked" stripe and associated with same number of fibrous tracts that extended along cell almost from end to end; left-most four or five folds and their associated fibers bent to right anteriorly; these formed hook-like cap and sub-apical depression below (Figs 1J, 3B, C). Remaining folds extended from this depression to posterior end of body. Oral cavity located in in anterior quarter of cell (Figs 1J, 2O, P). A lip-like structure on right side of oral cavity, and 13–29 right kineties ended here; consequently, lip-like region covered with dense cilia (Figs 1A–F, H, 2A, B, O, R, green region). Cytostome elliptical in outline and positioned at about anterior one third of cell, beneath depression of oral cavity (Figs 1J, 2B, O). Cytoplasm colorless, filled with a few lipid droplets and numerous food vacuoles containing unidentified amorphous inclusions in posterior end of cell. Contractile vacuole not detected.

Single macronucleus heteromerous and ovoid, about 35 × 20 μm after protargol impregnation, located in mid-body (Figs 1I, 2M). Micronucleus not detected. A prominent podite broadly cone-shaped, located at posterior end of cell (Figs 1A, H, I, 3A, J), about 10 μm in length *in vivo* (2A, F). Podite containing bifurcated secretory organelle which has an opening (0.5–1.0 μm across) at tip; obvious attachment thread (> 100 μm long) secreted from podite opening, forming strong connection with substrate (Figs 1A, 2E). Ciliates usually attached to surface of flocs of exfoliated epithelial tissue using podite and attachment thread. Cells tending to rotate through flocs of epithelial tissue.

Ciliary pattern (Figs 1H, I, J, 2F–R) comprising 49–79 somatic kineties, including 37–69 right and 7–13 left kineties. According to their starting position, right kineties including three parts: 1) right part of right kineties originated from right of circumoral kineties and these kineties on ventral side, with posterior ends gradually shortened from right to left (Fig. 1J); 2) middle part of right kineties originated from right of cell apex on ventral side and extending onto dorsal surface, and then posteriorly terminating at a level near podite (Fig. 1I, J); and 3) left part of right kineties located at cell apex on

For Review Only

dorsal side, and posteriorly extending to podite, with some extending onto left field on ventral side (Fig. 1H, I). Left kineties densely arranged, located on left margin of oral cavity. These kineties similar in length, and posteriorly ended in anterior quarter of cell (Figs 1J, 2O, Q, R). Four kinetofragments located slightly below mid-body on left margin of right kineties (Figs 1H, 2F). Equatorial fragment composed of 5-28 kinetosomes, positioned next to the middle part of the rightmost right kinety (Fig. 2K, L).

Oral ciliature composed of a tiny preoral kinety (~2 μm long) and two parallel circumoral kineties (~20 μm long) (Figs 1G, J, 2O, P, R, 3D, G); the former located on anterior-right of cavity, and the latter at mid of cavity. Anterior ends of circumoral kineties close to preoral kinety (Figs 1G, J, 2R). Cytopharynx reinforced by argentophilic fibers and extended to mid-body with posterior end obviously curved (Fig. 2P); no nematodesmal rods found.

Fine structures. Each of the circumoral kineties was composed of monokinetids (Fig. 4E). The cytopharyngeal tube consisted of ~180 cytostomal lamellae (Fig. 4A, B, D), which were bar-like and oriented obliquely to the center of the tube, forming an enclosed circle when viewed in cross sections. These lamellae were possibly heterogenous, as speculated from the morphology shown in cross sections: about two thirds of them were thinner in their distal ends, while the others were of uniform thickness (Fig. 4B, D).

The pellicle can be recognized as a ciliated area and non-ciliated stripe in both SEM prepared specimens and TEM sections. In the ciliated area the pellicular ridges were arranged intrakinetally (Fig. 3H, I). Each ridge contained a row of postciliary microtubules (Fig. 4C). Parasomal sacs occurred right of kinetosomes at the base of pellicular ridge (Fig. 4C). In the non-ciliated area, the pellicular folds were ~2 μm high containing four or five (mostly five) strata of microtubules beneath the pellicle (Figs 4H, I, 5), which corresponded with the fibrous tracts revealed after protargol staining (Figs 1J, 2R). The microtubules were highly organized: each stratum was arranged in an arch shape, extending with the same curve of the margin of the pellicular fold; each stratum contained several unequal sized fragments, which were always two layered but with different numbers of microtubules (Fig. 5). Pellicular pores occurred in the bases of grooves between the pellicular folds and were evenly separated, as revealed by SEM (Fig. 3E, F). In TEM, sacs (< 1 μm at their widest) regularly occurred beneath the pellicle of each groove, some of which contained materials and even opened toward the outside (Fig. 4F–I). There were often rich cytoplasmic vesicles containing granular material beneath the folds and near the secretory sacs (Figs 4I, 5). These results suggest a secretory system composed of the cytoplasmic vesicles, sacs and pellicular pores (Fig. 5). Mitochondria occurred mainly in the cytoplasm of the cortex area (Fig. 4C, G). Cytoplasm also contained food vacuoles encasing various food granules of different electron-density (Fig. 4A).

For Review Only

GENUS PLANILAMIA MA ET AL., 2006

PLANILAMINA OVATA MA ET AL., 2006 (Figs 6–7, Table 1)

Improved diagnosis. Cell size 35–80 × 30–50 μm *in vivo*; laterally flattened, discoid or ovate in side view; deep oral cavity composed of a preoral kinety (rarely two), two circumoral kineties, and 7–13 infundibular kineties; no nematodesmal rods; 38–58 right kineties, 3–4 left kineties; four kinetofragments located in the left ahead of the podite; macronucleus ovoid; one contractile vacuole adjacent to cytostome.

Host. *Delphinapterus leucas* Pallas, 1776 (beluga whale).

Voucher material. Four slides with protargol-stained specimens (indicated with a black circle of ink on each coverslip) have been deposited in the collection of Ningbo University (registration numbers: LJ-II-20170502-01, 02, 03, and 04).

General morphology and ciliary pattern of Ningbo population. Cell size 55–80 × 40–50 μm *in vivo*, and 50–80 × 32–47 μm after protargol staining. Body laterally flattened shape with a length-width ratio of about 3:2 in lateral view (Figs 6A, 7A). From lateral view, cell discoid or ovate in outline; anterior end slightly pointed and posterior margin broadly rounded (Fig. 6A, C). Dorsal margin of ciliated right region sculptured by C-shaped band (or groove) (Fig. 7A, M). This band extends from apex of cell to posterior end. Some long bands (23 out of 35 individuals observed) curve around the posterior end, and anteriorly onto left of podite. This structure is visible as a deep groove *in vivo*, and as an argentophilic band (AB) in protargol-impregnated specimens (Fig. 6D, E). Left surface not regular in shape (Figs 6B, 7B). Oral cavity broad and located at the anterior quarter of the cell. Cytostome located posteriorly in oral cavity (Figs 6F, 7G, I, M). Cytoplasm colorless, containing multiple food vacuoles consisting of unidentified amorphous material. Single contractile vacuole, up to 6 μm across, positioned in the left of mid-body in ventral view, contraction with an interval of 20–30 s; contractile vacuole pore located between second and third right kineties in mid-body (Fig. 6A, E).

Macronucleus ovoid and heteromerous, located in mid-body (Figs 6F, 7M). Micronucleus ellipsoid and adjacent to macronucleus (Fig. 6D). Podite broadly cone-shaped, situated on the posterior quarter of cell, about 4–6 μm in length and 3–8 μm across at the base (Figs 6A, E, 7A). Individuals often attached to substrate by podite and rotation through viscous medium with cilia beating in a regular pattern.

Cilia about 8 μm long *in vivo*. Ciliature as shown in Figs 6E, F, 7F–M. Kinetosomes in somatic kineties densely arranged. Somatic kineties divided into three parts, right, left and kinetofragments. Right field comprising 41–58 kineties; leftmost 15–25 relatively short, extending from level of oral field to level of podite; remaining kineties originated from apex of cell, and extending posteriorly to cell end and bending to left (Fig. 6E). Three to four left kineties located on left of oral cavity, originated

For Review Only

from near apex of cell and terminated posteriorly at level of posterior margin of cytostome, about two-fifths of cell length (Figs 6E, 7G, H). Four short kinetofragments located on anterior-left of podite and often curved to right. (Figs 6F, 7J, K, L). Equatorial fragment undetected.

Oral ciliature composed of a preoral kinety (seldom two), two parallel circumoral kineties and nine to thirteen infundibular kineties (Fig. 6F). Circumoral kineties located on anterior of cytostome (Figs 6F, 7I). Preoral kinety located on anterior-left of circumoral kineties, consisting of one or two closely set kinetosomes (Figs 6F, 7H). Infundibular kineties positioned in arc of circumoral kineties (Fig. 7H). Cytopharynx extending below mid-body and curved posteriorly; no nematodesmal rod found (Figs 6F, 7G, M).

MOLECULAR DATA AND PHYLOGENETIC POSITION (Figs 8–10)

The GenBank accession numbers, lengths, and G + C contents of sequences (SSU and LSU rDNA, and ITS1-5.8S-ITS2) of *Kyaroikeus paracetarius* sp. nov. and *Planilamina ovata* from this study are provided in Table 2. The topologies of the BI and ML trees were almost identical; thus, only the ML tree was presented here, with support values from both of the algorithms indicated on branches.

SSU rDNA (Figure 8). *Planilamina ovata* was sister to *Trochilia petrani* with low supporting values (ML/BI, 65%/0.80), and their branch then clustered with *Kyaroikeus paracetarius* sp. nov. with full support. Furthermore, the branch of *Trochilia*/*Kyaroikeus*/*Planilamina* clustered with *Microxysma* (ML/BI, 80%/1.00) and then with the core of Dysteriidae species represented by *Dysteria*, *Spirodysteria*, and *Mirodysteria*, with moderate support values (ML/BI, 78%/0.98).

ITS1-5.8S-ITS2 (Figure 9). *Planilamina ovata* clustered with *Kyaroikeus paracetarius* sp. nov. (ML/BI, 67%/0.82), forming a clade with *Dysteria derouxi* (ML/BI, 88%/0.97).

LSU rDNA (Figure 9). *Kyaroikeus paracetarius* sp. nov. clustered with *Planilamina ovata* with full support, and then this branch formed a clade with *Dysteria derouxi* with full support.

Concatenated genes (Figure 10). The phylogenetic tree based on the concatenated dataset was different from the SSU rDNA tree; i.e., *Kyaroikeus paracetarius* sp. nov., *Planilamina ovata* and *Trochilia petrani* grouped into one clade with 100 % bootstrap values in ML tree but were not resolved by BI. The families Chilodonellidae and Lynchellidae were located in different positions, and Lynchellidae was closer to Chlamydodontidae in concatenated gene tree, while Chilodonellidae was closer to Chlamydodontidae, and Lynchellidae was on a peripheral position in SSU rDNA tree.

DISCUSSION

For Review Only

As indicated in the Methods and Materials, the beluga whale was maintained in a closed, carefully controlled environment. It is unlikely that the ciliates arrived through contamination of the system. Rather, as the beluga whale was born in the wild, and the ciliates were found even when it was healthy, we suggest that there are natural, low-level populations of ciliates in most whales that only become abundant when they are unhealthy. The reports of ciliates from the respiratory tracts of other whales support this (Lair *et al*., 2016; Ma *et al*., 2006; McFee & Lipscomb, 2009).

Several studies suggest that ciliates infesting whale respiratory tracts belong to two genera, *Kyaroikeus* and *Planilamina*, within which species are morphologically adapted to a parasitic life (Ma *et al*., 2006; Sniezek *et al*., 1995). However, because of the lack of molecular and morphological information, there remains a poor understanding of the phylogenetic positions, evolutionary origin, and the adaptive modifications of these species. Here, we applied state-of-the-art approaches (Warren *et al*., 2017) to recognize and characterize two species found in an infected beluga whale: *K. paracetarius* sp. nov. and *P. ovata* Ma *et al*., 2006; considering their exceptionally high abundance when the host was unhealthy, we consider these species to be parasites. Then, based on our phylogenetic and morphological analyses, we suggest revisions to the systematic positions of the two parasitic genera and then speculate on how they may have invaded the host and their morphological adaptations to residing in the blow-hole of beluga whales.

Beyond these fundamental aspects of phylogeny and adaptation, we suggest that a good appreciation of the biology of this potential pathogen may be useful to understand disease. For instance, information on phylogeny and evolutionary origin can provide insights into other potential pathogens and adaptive features associated with lineages. Existing knowledge of near phylogenic neighbors may also offer insights into key functions of pathogens. Clearly, also understanding how pathogens have adapted to a parasitic life allows researchers to consider how they act and how they may be prevented from acting. We hope, therefore, that our work will be wide reaching in its impact.

ESTABLISHMENT OF THE NEW KYAROIKEUS SPECIES

Sniezek *et al*. (1995) established the genus *Kyaroikeus* by describing the type species *K. cetarius.* The main features of our isolate fit the diagnosis of the genus *Kyaroikeus*, supporting the genetic placement of the new species. However, our organism differs from its only congener *K. cetarius* in two key attributes: a larger number of right somatic kineties (37–69 [arithmetic mean 66] vs. 44–51 [arithmetic mean 48] in *K. cetarius*) and, critically, the number of left kineties, considered stable in cyrtophorid ciliates (our isolate has 7–13 left kineties [arithmetic mean 10], while *K. cetarius* has only 4). Although there was variation in the number of right and left kineties in *K. paracetarius* sp. nov., there was no clear correlation between these, nor did they appear to be correlated with cell size (Supplementary Figure S3), suggesting that the variation was random Accordingly, we have established the species *K. paracetarius* sp. nov.

For Review Only

COMMENTS ON *PLANILAMINA OVATA*

Planilamina ovata was first collected from Atlantic bottlenose dolphins and false killer whale in USA and described by Ma *et al*. (2006) using the protargol staining method. The Ningbo population closely matches the original description in body shape, living and stained morphological features, except for some minor differences: the Ningbo population has a larger cell size *in vivo* (50–80 × 32–47 μm vs. 28–65 × 20–43 μm) and has a wider range number of right kineties (41-58 vs. 41-51). These are minor differences, and the ranges overlap, so we conclude that our identification of Ningbo population is correct.

THE PARASITES AROSE FROM A DYSTERIIDAE ANCESTOR

Sniezek & Coats (1996) established the family Kyaroikeidae with *Kyaroikeus* as the type genus, placed the family in the order Cyrtophorida, and according to their morphogenesis suggested this family to be closely related to the family Dysteriidae, which is currently composed only of free-living species. Later, Ma *et al*. (2006) erected the parasitic genus *Planilamina* and assigned it to the Kyaroikeidae. Our SSU rDNA-based phylogenetic results support that the two genera belong to the subclass Cyrtophoria (Fig. 8), and the general topologies of the subclass match the results of others (e.g., Chen *et al*., 2016; Gao *et al*., 2012; Qu *et al*., 2017). However, addition of our new gene sequences questions the validity of the Kyaroikeidae, as the clade represented by this family includes both parasitic and free-living genera and falls within the Dysteriidae (Fig. 8). This molecular clustering is also reflected by morphological characteristics; i.e., the kyaroikeids and dysteriids share a similar ciliary pattern in that they both include highly degenerated left kineties in the front-left of the cell and short post oral kineties in mid-body (Figs 1A, 6A; Lynn 2008).

The two parasitic genera, representing the current Kyaroikeidae, do exhibit unique features (i.e., a large number of right kineties, large ciliated regions, and dense cilia, Figs 1H, I, 6E). However, the free-living genus *Trochilia*, which clusters with the two parasitic ciliates, is morphologically more like other free-living members of the Dysteriidae (see Fig. 4K in Liu *et al*., 2017). We suggest that the unique structures (i.e., dense cilia, pellicular fold contained 5 to 6 layers, prominent oral cavity, pellicular pores) of the parasites are convergent and has arisen through adaptation to their environment (see next section). Thus, we propose that the family Kyaroikeidae is invalid and suggest that, for now, it should be retained, but only as a sub-family within the Dysteriidae.

Regardless of the formal position of the Kyaroikeidae, our phylogenetic analysis clearly indicates that the parasitic genera *Planilamina* and *Kyaroikeus* evolved from a free-living Dysteriidae-like ancestor. Furthermore, the close association of the free-living genus *Trochilia* to the parasitic genus *Planilamina* (Fig. 8) implies that parasitism may have arisen more than once. The free-living Dysteriidae tend to occupy periphytic environments, including sediments, sea ice, and associations with marine algae (Meng *et al*., 2018; Petz *et al*., 1995; Song & Wilbert, 2000). Marine mammals and

For Review Only

specifically beluga whales will roll in sediments and rub against hard surfaces to remove dead skin and ectoparasites (Smith *et al*., 1992). This may have allowed invasion of free-living Dysteriidae into their respiratory system, where they adapted to live permanently. Inevitably, as more parasitic and free-living taxa in these clades are recognized, our predictions will be more rigorously evaluated.

MORPHOLOGICAL MODIFICATIONS FOR A PARASITIC LIFE

Kyaroikeus paracetarius sp. nov. and *Planilamina ovata* appear to be obligatory parasites as they could not live freely in water (see Methods), and we suggest that they have morphologically adapted to this life through structures that: 1) increase movement through viscous mucus; 2) improve ingestion of cellular material; and 3) adhere to flocs of mucus and facilitate food uptake. We outline these below and suggest they are worthy of further investigation.

Increased movement through viscous mucus. The free-living dysteriid species have few, fragmented right kineties (at most 13 rows in Dysteriidae spp. and only 4 in *Trochilia* spp.), and these are constrained in a narrow ventral groove with sparsely distributed cilia and weak microtubules structure (Qu *et al*., 2015). In contrast, the two parasitic species have many non-fragmented right kineties that occupy a substantial part of the cell surface (Figs 1H-J, 6E); they also are densely ciliated. We suggest that these modifications contribute to the motility of the organisms in viscous mucus. Moreover, the cortex of dorsal surface is compressed into stripes, and under these pellicular folds there is a unique microtubular structure (outlined below and described by Sniezek *et al*., 1995). In several groups of ciliates, microtubules that run longitudinally under the pellicle allow cells to maintain and change cell shape (Lynn, 2008). Generally, there is only one or two layers and several bundles of these microtubules (Calvo *et al*., 1986; Kurth & Bardele, 2001; Wirnsberger-Aescht *et al*., 1989). However, in *K. paracetarius* sp. nov., each pellicular fold contained 5 to 6 layers and multiple bundles (Fig. 4H and Fig. 5), suggesting a greater role in movement, possibly allowing cells to penetrate in the mucus. (Supplementary Video S1).

Improved ingestion of cellular material. Compared to the free-living dysteriids, the two parasitic genera have a pronounced oral cavity. The oral region reflects functional diversity among ciliates (Eisler, 1992). For members of the free-living dysteriids, their oral region is prominent with strong nematodesmal rods, allowing them to capture particulate food (Foissner *et al*., 1991; Qu *et al*., 2015). In contrast, the two parasitic species have densely arranged cilia near the oral area that are likely used to transport large volumes of liquid, moving large food particles (exfoliated epithelial cells) towards the cytostome into their deep oral cavity (Figs 1E, F, 6A).

Adhering to mucus and improved food uptake. Pellicular pores that occur in the pellicle of sessile peritrich ciliates (e.g., Finley *et al*., 1972; Lom & Corliss, 1968) are considered to be sites of mucus material secretion, lorica-formation, and stalk-production (Bauer-Nebelsick *et al*., 1996; Lynn, 2008); to our knowledge such pores are not reported in the free-living dysteriids. However, they are also found in the non-ciliated area and the podite of an ectoparasite ciliate (*Brooklynella hostilis*) of marine fishes,

For Review Only

(Lom & Corliss, 1971). Similar structures occur in *Cryptocaryon irritans,* a parasite ciliate causing white spot disease of marine fishes, where pellicular openings are connected to small vesicles and may serve in enzyme excretion or food uptake (Matthews *et al*., 1993). We observed pellicular pores in *K. paracetarius* sp. nov. (Figs 3E, F, 4H, 5) and suggest that they may function in secretion of mucus material (for adhesion) or secretion of enzymes (aiding in feeding).

CONCLUSION

In this study we provide an evaluation of the occurrence and abundance of two ciliates that appear to be parasites (but may admittedly be opportunistic endocommensals) within the respiratory tract of a beluga whale. Our efforts to culture the ciliates were unfortunately not successful. We suggest that continued work now explores the protozoa in the mucus of whales, evaluating changes in abundance and making further efforts to culture taxa to reveal their life cycles. Furthermore, now that we have provided substantial molecular data for these taxa, we encourage the development of barcoding approaches (Zhao *et al*., 2018), to allow rapid assessment of these taxa, on a wider scale.

For Review Only

REFERENCES

Bauer-Nebelsick M, Bardele CF, Ott JA. 1996. Electron microscopic studies on *Zoothamnium niveum* (Hemprich & Ehrenberg, 1831) Ehrenberg 1838 (Oligohymenophora, Peritrichida), a ciliate with ectosymbiotic, chemoautotrophic bacteria. *European Journal of Protistology* **32:** 202–215.

Calvo P, Torres A, Fedriani C, Rios RM, Silva JP. 1986. Ultrastructure chez *Histriculus similis* (Cilié hypotriche). *Acta Protozoologica* **25:** 23–32.

Chen X, Pan H, Huang J, Warren A, Al-Farraj SA, Gao S. 2016. New considerations on the phylogeny of cyrtophorian ciliates (Protozoa, Ciliophora): expanded sampling to understand their evolutionary relationships. *Zoologica Scripta* **45:** 334–348.

Choi YK, Kang MS, Sohn HR, Kim DY. 2003. Disseminated ciliated protozoan infection in a Pacific dolphin (*Tursiops gill*). *Veterinary Record* **153:** 714–715.

Eisler K. 1992. Somatic kineties or paroral membrane: Which came first in ciliate evolution? *BioSystems* **26:** 239–254.

Finley HE, Ranganathan VS, Small EB. 1972. Examination of the peritrich ciliate *Telotrochidium* by scanning electron microscopy. *Transactions of the American Microscopical Society* **91:** 492–501.

Foissner W, Blatterer H, Berger H, Kohmann F. 1991. Taxonomische und ökologische Revision der Ciliaten des Saprobiensystems – Band I: Cyrtophorida, Oligotrichida, Hypotrichia, Colpodea. *Informationsberichte des Bayer. Landesamtes für Wasserwirtschaft* **1/91:** 1–478.

Gao F, Warren A, Zhang Q, Gong J, Miao M, Sun P, Xu D, Huang J, Yi Z, Song W. 2016. The all-data-based evolutionary hypothesis of ciliated protists with a revised classification of the phylum Ciliophora (Eukaryota, Alveolata). *Scientific Reports* **6:** 24874.

Gao S, Huang J, Li J, Song W. 2012. Molecular phylogeny of the cyrtophorid ciliates (Protozoa, Ciliophora, Phyllopharyngea). *PLoS One* **7:** e33198.

Gulland MD, Dierauf A, Whitman L. 2018. Protozoan parasites of marine mammals. In: Miller M, eds. *CRC Handbook of Marine Mammal Medicine*, 3nd ed. Boca Raton: CRC Press, 425–470.

Hall TA. 1999. BioEdit: a user-friendly biological sequence alignment editor and analysis program for Windows 95/98/NT. *Nucleic Acids Symposium Series* **41:** 95–98.

Hermosilla C, Silva LMR, Kleinertz S, Prieto R, Silva MA, Taubert A. 2016. Endoparasite survey of free-swimming baleen whales (*Balaenoptera musculus*, *B. physalus*, *B. borealis*) and sperm whales (*Physeter macrocephalus*) using non/minimally invasive methods. *Parasitology Research* **115:** 889–896.

Hermosilla C, Silva LMR, Prieto R, Kleinertz S, Taubert A, Silva MA. 2015. Endo- and ectoparasites of large whales (Cetartiodactyla: Balaenopteridae, Physeteridae): Overcoming difficulties in obtaining appropriate samples by non- and minimally-invasive methods. *International Journal for Parasitology: Parasites and Wildlife* **4:** 414–420.

Hu X, Lin X, Song W. 2019. *Ciliate Atlas: Species Found in the South China Sea*. Beijing: Science

For Review Only

Press.

Kurth T, Bardele CF. 2001. Fine structure of the cyrtophorid ciliate *Chlamydodon mnemosyne* Ehrenberg, 1837. *Acta Protozoologica* **40:** 33–48.

Lair S, Measures LN, Martineau D. 2016. Pathologic findings and trends in mortality in the beluga (*Delphinapterus leucas*) population of the St Lawrence Estuary, Quebec, Canada, from 1983 to 2012. *Veterinary Pathology* **53:** 22–36.

Liu W, Jiang J, Xu Y, Pan X, Qu Z, Luo X, El-Serehy H, Warren A, Ma H, Pan H. 2017. Diversity of free-living marine ciliates (Alveolata, Ciliophora): Faunal studies in coastal waters of China during the years 2011-2016. *European Journal of Protistology* **61:** 424–438.

Lom J, Corliss JO. 1968. Observations on the fine structure of two species of the peritrich ciliate genus *Scyphidia* and on their mode of attachment to their host. *Transactions of the American Microscopical Society* **87:** 493–509.

Lom J, Corliss JO. 1971. Morphogenesis and cortical ultrastructure of *Brooklynella hostilis*, a dysteriid ciliate ectoparasitic on marine fishes. *Journal of Protozoology* **18:** 261–281.

Lynn DH. 2008. *The ciliated Protozoa, characterization, classification, and guide to the literature.* Dordrecht: Springer.

Lynn DH, Corliss JO. 1991. Ciliophora. In: Harrison FW, Corliss JO, eds. *Microscopic anatomy of invertebrates*. New York: Wiley-Liss, 333–467.

Ma H, Overstreet RM, Sniezek JH, Solangi M, Wayne Coats D. 2006. Two new species of symbiotic ciliates from the respiratory tract of cetaceans with establishment of the new genus *Planilamina* n. gen. (Dysteriida, Kyaroikeidae). *Journal of Eukaryotic Microbiology* **53:** 407–419.

Ma R, Ni B, Fan X, Warren A, Yin F, Gu F. 2016. Ultrastructure observation on the cells at different life history stages of *Cryptocaryon irritans* (Ciliophora: Prostomatea), a parasitic ciliate of marine fishes. *Parasitology* 143: 1479–1489.

Matthews BF, Matthews RA, Burgess PJ. 1993. *Cryptocaryon irritans* Brown, 1951 (Ichthyophthiriidae): the ultrastructure of the somatic cortex throughout the life cycle. *Journal of Fish Diseases* **16:** 339–349.

McFee WE, Lipscomb TP. 2009. Major pathologic findings and probable causes of mortality in bottlenose dolphins stranded in South Carolina from 1993 to 2006. *Journal of Wildlife Diseases* **45:** 575–593.

Medlin L, Elwood HJ, Stickel S, Sogin ML. 1988. The characterization of enzymatically amplified eukaryotic 16S-like rRNA-coding regions. *Gene* **71:** 491–499.

Meng Z, Xu K, Dai R, Warren A. 2018. Benthic ciliate diversity and community composition along water depth gradients: a comparison between the intertidal and offshore areas. *European Journal of Protistology* **65:** 31–41.

Moreira D, von der Heyden S, Bass D, López-García P, Chao E, Cavalier-Smith T. 2007. Global eukaryote phylogeny: Combined small- and large-subunit ribosomal DNA trees support

For Review Only

monophyly of Rhizaria, Retaria and Excavata. *Molecular Phylogenetics and Evolution* **44:** 255–266.

Norman SA, Goertz CE, Burek KA, Quakenbush LT, Cornick LA, Romano TA, Spoon T, Miller W, Beckett LA, Hobbs RC. 2012. Seasonal hematology and serum chemistry of wild beluga whales (*Delphinapterus leucas*) in Bristol Bay, Alaska, USA. *Journal of Wildlife Diseases* **48:** 21–32.

Nylander JA. 2004. *MrModeltest v2*. Distributed by the author. Evolutionary Biology Center, Uppsala University.

Page RDM. 1996. Treeview: an application to display phylogenetic trees on personal computers. *Computer Applications in the Biosciences* **12:** 357–358.

Pan X, Bourland WA, Song WB. 2013. Protargol synthesis an in-house protocol. Journal of Eukaryotic Microbiology **60:** 609–614.

Petz W, Song W, Wilbert N. 1995. Taxonomy and ecology of the ciliate fauna (Protozoa, Ciliophora) in the endopagial and pelagial of the Weddel Sea, Antarctica. *Stapfia* 40: 1–223.

Posada D, Crandall KA. 1998. Modeltest: testing the model of DNA substitution. *Bioinformatics* **14:** 817–818.

Poynton SL, Whitaker BR, Heinrich AB. 2001. A novel trypanoplasm-like flagellate *Jarrellia atramenti* n. g., n. sp. (Kinetoplastida: Bodonidae) and ciliates from the blowhole of a stranded pygmy sperm whale *Kogia breviceps* (Physeteridae): morphology, life cycle and potential pathogenicity. *Diseases of Aquatic Organisms* **44:** 191–201.

Qu Z, Ma H, Al-Farraj SA, Lin X, Hu X. 2017. Morphology and molecular phylogeny of *Aegyria foissneri* sp. n. and *Lynchella minuta* sp. n. (Ciliophora, Cyrtophoria) from brackish waters of southern China. *European Journal of Protistology* **57:** 50–60.

Qu Z, Wang C, Gao F, Li J, Al-Rasheid KAS, Hu X. 2015. Taxonomic studies on seven species of *Dysteria* (Ciliophora, Cyrtophoria), including a description of *Dysteria paraprocera* sp. n. *European Journal of Protistology* **51:** 241–258.

Ronquist F, Huelsenbeck JP. 2003. MrBayes 3: Bayesian phylogenetic inference under mixed models. *Bioinformatics* **19:** 1572–1574.

Smith TG, St. Aubin DJ, Hammill MO. 1992. Rubbing behaviour of belugas, *Delphinapterus leucas*, in a high Arctic estuary. *Canadian Journal of Zoology* **70:** 2405–2409.

Sniezek JH, Coats DW. 1996. Stomatogenesis in *Kyaroikeus cetarius* (Dysteriina, Kyaroikeidae, n. fam.): clues to its systematic placement. *Journal of Eukaryotic Microbiology* **43:** 113–119.

Sniezek JH, Coats DW, Small EB. 1995. *Kyaroikeus cetarius* n. g., n. sp.: a parasitic ciliate from the respiratory tract of odonticete cetacea. *Journal of Eukaryotic Microbiology* **42:** 260–268.

Song W, Warren A, Hu X. 2009. *Free-living Ciliates in the Bohai and Yellow Seas, China.* Beijing: Science Press.

Song W, Wilbert N. 2000. Ciliates from Antarctic sea ice. *Polar Biology* **23:** 212–222.

For Review Only

Stamatakis A, Hoover P, Rougemont J. 2008. A rapid bootstrap algorithm for the RAxML web servers. *Systematic Biology* **57:** 758–771.

Tamura K, Peterson D, Peterson N, Stecher G, Nei M, Kumar S. 2011. MEGA5: molecular evolutionary genetics analysis using maximum likelihood, evolutionary distance, and maximum parsimony methods. *Molecular Biology and Evolution* **28:** 2731–2739.

Wang P, Wang Y, Wang C, Zhang T, Al-Farraj SA, Gao F. 2017. Further consideration on the phylogeny of the Ciliophora: Analyses using both mitochondrial and nuclear data with focus on the extremely confused class Phyllopharyngea. *Molecular Phylogenetics and Evolution* **112:** 96–106.

Warren A, Patterson DJ, Dunthorn M, Clamp JC, Achilles-Day UEM, Aescht E, Al-Farraj SA, Al-Quraishy S, Al-Rasheid K, Carr M, Day JG, Dellinger M, El-Serehy HA, Fan Y, Gao F, Gao S, Gong J, Gupta R, Hu X, Kamra K, Langlois G, Lin X, Lipscomb D, Lobban CS, Luporini P, Lynn DH, Ma H, Macek M, Mackenzie-Dodds J, Makhija S, Mansergh RI, Martín-Cereceda M, McMiller N, Montagnes DJS, Nikolaeva S, Ong'ondo GO, Pérez-Uz B, Purushothaman J, Quintela-Alonso P, Rotterová J, Santoferrara L, Shao C, Shen Z, Shi X, Song W, Stoeck T, La Terza A, Vallesi A, Wang M, Weisse T, Wiackowski K, Wu L, Xu K, Yi Z, Zufall R, Agatha S. 2017. Beyond the "code": a guide to the description and documentation of biodiversity in ciliated protists (Alveolata, Ciliophora). *Journal of Eukaryotic Microbiology* **64:** 539–554.

Wilbert N. 1975. Eine verbesserte Technik der Protargolimprägnation für Ciliaten. *Mikrokosmos* **64:** 171–179.

Wirnsberger-Aescht E, Foissner W, Foissner I. 1989. Morphogenesis and ultrastructure of the soil ciliate *Engelmanniella mobilis* (Ciliophora, Hypotrichida). *European Journal of Protistology* **24:** 354–368.

Yi Z, Song W, Clamp JC, Chen Z, Gao S, Zhang Q. 2009. Reconsideration of systematic relationships within the order Euplotida (Protista, Ciliophora) using new sequences of the gene coding for small-subunit rRNA and testing the use of combined data sets to construct phylogenies of the *Diophrys*-complex. *Molecular Phylogenetics and Evolution* **50:** 599–607.

Zhao Y, Yi Z, Gentekaki E, Zhan A, Al-Farraj SA, Song W. 2016. Utility of combining morphological characters, nuclear and mitochondrial genes: an attempt to resolve the conflicts of species identification for ciliated protists. *Molecular Phylogenetics and Evolution* **94:** 718–729.

Zhao Y, Yi Z, Warren A, Song W. 2018. Species delimitation for the molecular taxonomy and ecology of the widely distributed microbial eukaryote genus *Euplotes* (Alveolata, Ciliophora). *Proceedings of the Royal Society B: Biological Sciences* **285:** 20172159.

For Review Only

LEGENDS

Figure 1. *Kyaroikeus paracetarius* sp. nov. from life (A–D) and after protargol impregnation (E–J). A. Ventral view to show the body shape, densely arranged cilia, lip-like structure on the right side of oral cavity (green region), the podite, and the attachment thread. B-D. Variants of cell shape. E. The oral region: the blue area indicates the kineties of right field on cell apex and the arrowhead indicates the lip-like structure. F. The cytostome and the circumoral kineties (brown lines). G. The oral region, to show the preoral kinety (arrowhead) and circumoral kineties. H, I. Ventral (H) and dorsal (I) views of infraciliature: the arrowhead indicates the lip-like structure and the arrow indicates the equatorial fragment. J. Enlargement of the anterior ventral part of infraciliature to show details of the oral structure, right and left somatic kineties, and non-ciliated stripes. Abbreviations: C, cytostome; Co, circumoral kineties; FT, fibrous tracts; KF, kinetofragments; LF, left field; Ma, macronucleus; NS, non-ciliated stripe; P, podite; Po, preoral kinety; RF, right field; T, attachment thread. Scale bars = 60 μm (A, H–J).

Figure 2. Photomicrographs of *Kyaroikeus paracetarius* sp. nov. from life (A–E) and after protargol impregnation (F–R). A. Ventral view of a representative individual; the green region is the lip-like structure on the right side of oral cavity. B. Ventral view of the anterior, to show the oral area, with the arrowhead indicating the cytopharynx. C. Enlargement of the anterior of the cell. D. Anterior of the cell, with the arrowhead indicating the non-ciliated stripe. E. Posterior of the cell, with the arrow indicating the podite and arrowhead indicating the attachment thread. F, G. Ventral and dorsal views of the infraciliature, with the arrowhead indicating the kinetofragments, the arrow indicating the podite, and the red dots outlining the non-ciliated area. H–J. Mid-ventral region of several specimen with different shapes and number of kinetofragments, normal individual with four lines (I), individuals in early stage of fission with more lines (I, J). K, L. Equatorial fragment (arrowheads), next to the middle part of the rightmost right kinety. M. The heteromeric macronucleus. N. The podite. O, P. Enlargement of the oral region, with the arrows indicating the circumoral kineties and the arrowheads indicating the preoral kinety. Q. Dorsal view of the anterior, showing the densely arranged right kineties (RK) and left kineties (LK). R. Enlargement of the oral region, with the arrow indicating the pellicular fold, the arrowhead indicating the preoral kinety, and green region highlighting the lip-like structure. Abbreviations: C, cytostome; Co, circumoral kineties; FT, fibrous tracts; LF, left field; Ma, macronucleus; RF, right field. Scale bars = 60 μm (A–C, F, G) or 30 μm (O–R).

Figure 3. Scanning electron micrographs of *Kyaroikeus paracetarius* sp. nov. A. The general body shape and the podite in posterior end (white circle). B, C. Anterior portion of cell, showing the pellicular fold in the non-ciliated stripe, which hooks over the anterior end. D, G. Oral area, with arrows indicating the circumoral kineties observed in different individuals. E, F. The non-ciliated stripe, with the arrowheads indicating the pellicular pores, which occur in the grooves between the pellicular folds. H,

For Review Only

I. A de-ciliated specimen, showing the densely arranged kinetosomes (arrowheads) of ciliary rows and the pellicular ridges (arrow) in the right field of cell. J. The podite, indicating the secretion pore (arrow). Abbreviations: NS, non-ciliated stripe; P, podite. Scale bars = 50 μm (A), 10 μm (B), 5 μm (C, D, G, J), or 2 μm (E, F, H, I).

Figure 4. Transmission electron micrographs of *Kyaroikeus paracetarius* sp. nov. A. Cross section showing the non-ciliated stripe, ciliated area (the surface part other than NF), cytopharyngeal tube, and a food vacuole. B, D. Details of cytopharyngeal tube, which is a flat vesicle. The arrows indicate the microtubule sheets with thinner ends, the double arrowhead indicates one of even thickness, and arrowhead indicates the narrow space of cytopharyngeal tube. C. The pellicular ridges which were present between ciliary rows and supported by postciliary microtubules, and the parasomal sacs. E. The oral region, showing the two circumoral kineties that were composed of a single row of kinetosomes. F–I. The pellicular folds in the non-ciliated stripe, arrows indicate the sacs regularly occurred beneath the pellicle of each groove, arrowheads mark the sacs which contained materials or connected with outside, double-arrowhead marks the rich cytoplasmic vesicles in the cytoplasm beneath the folds and near the sacs. Abbreviations: Co, circumoral kineties; CT, cytopharyngeal tube; FV, food vacuole; MIT, mitochondria; NS, non-ciliated stripe; PCMT, postciliary microtubules; PS, parasomal sacs; Scale bars = 10 μm (A), 0.5 μm (B–D, H, I), or 2 μm (E, G), 1 μm (F).

Figure 5. The cortex of the non-ciliated stripe of *Kyaroikeus paracetarius* sp. nov., showing the arrangement of microtubules and a proposed material secretion system containing cytoplasmic vesicles, sacs, and pellicular pores.

Figure 6. *Planilamina ovata* from life (A–C) and after protargol impregnation (D–F). A. Right lateral view of a typical individual. B. Left lateral view; arrowhead points to the anterior kineties of right field turning over onto dorsal side. C. Ventral view; arrowhead points to the anterior kineties of right field turning over onto ventral side. D. Right lateral view, showing the argentophilic band, macronucleus and micronucleus. E. Right lateral view of ciliature; arrow indicates the contractile vacuole pore. F. Left lateral view, showing the oral region, kinetofragments and macronucleus. Abbreviations: AB, argentophilic band; C, cytopharynx; Co, circumoral kineties; CV, contractile vacuole; I, infundibular kineties; KF, kinetofragments; LF, left field; Ma, macronucleus; Mi, micronucleus; P, podite; Po, preoral kineties; RF, right field. Scale bars = 25 μm.

Figure 7. *Planilamina ovata* from life (A–E) and after protargol impregnation (F–M). A. Right lateral view of a representative individual; arrow indicates the podite, and arrowheads indicate the C-shaped bright groove B. Left lateral view; arrow points to the anterior kineties of right field turning over to dorsal side, and arrowheads show the short grooves on surface. C. Ventral view; arrowhead indicates

For Review Only

oral region. D, E. Arrowheads indicate the podite. F. Showing the podite (arrow). G. Showing the oral region; arrow indicates infundibular kineties, double arrowheads indicate circumoral kineties, and arrowhead indicates the contractile vacuole pore. H, I. Showing the oral region; arrow indicates infundibular kineties, arrowheads indicate preoral kineties, and double arrowheads indicate circumoral kineties. J–L. Specimen in different shape and numbers of kinetofragments (arrowheads); arrows indicate the podite. M. Right lateral view of ciliature; arrow indicates argentophilic band, and arrowhead indicates cytopharynx. Abbreviations: C, cytopharynx; LF, left field; Ma, macronucleus; RF, right field. Scale bars = 25 μm (A–C, M).

Figure 8. Phylogenetic tree inferred from SSU rDNA sequences, revealing the position of *Kyaroikeus paracetarius* sp. nov. and *Planilamina ovata* (red font). Numbers near branches represent posterior probabilities for BI and bootstrap values for ML. Asterisks indicate topologies that differ between the ML and BI phylogenies. Fully supported (100/1.00) branches are marked with solid circles. The scale bar corresponds to five substitutions per 100 nucleotide sites.

Figure 9. Phylogenetic trees inferred from ITS1-5.8S-ITS2 and LSU rDNA sequences, revealing the position of *Kyaroikeus paracetarius* sp. nov. and *Planilamina ovata* (red font). Numbers near branches represent posterior probabilities for BI and bootstrap values for ML. Asterisks indicate topologies that differ between the ML and BI phylogenies. Fully supported (100/1.00) branches are marked with solid circles. The scale bar corresponds to five substitutions per 100 nucleotide sites.

Figure 10. Phylogenetic tree inferred from the concatenated genes (SSU rDNA, ITS1-5.8S-ITS2, LSU rDNA), revealing the position of *Kyaroikeus paracetarius* sp. nov. and *Planilamina ovata* (red font). Numbers near branches represent posterior probabilities for BI and bootstrap values for ML. Asterisks indicate topologies that differ between the ML and BI phylogenies. Fully supported (100/1.00) branches are marked with solid circles. The scale bar corresponds to five substitutions per 100 nucleotide sites.

For Review Only

Table 1. Morphometric data of *Kyaroikeus paracetarius* sp. nov. (upper line) and *Planilamina ovata* (lower line) based on Protargol-stained specimens.

character	Max	Mix	Mean	Median	SD	SE	CV	*n*
Body length (μm)	364.0	150.0	210.3	203.5	47.5	9.3	22.6	26
	80.0	50.0	61.6	61.0	7.7	1.5	12.4	26
Body width (μm)	77.0	34.0	48.4	47.0	10.5	2.1	21.7	26
	47.0	32.0	38.2	37.5	4.2	0.8	11.1	26
Macronucleus, length (μm)	75.0	22.0	37.8	34.0	12.0	2.4	31.8	26
	27.0	12.0	18.1	18.0	3.3	0.7	18.3	26
Macronucleus, width (μm)	32.0	13.0	19.5	19.0	4.2	0.8	21.6	26
	20.0	9.0	13.8	13.5	3.4	0.7	24.8	26
Podite, length (μm)	13.0	6.0	10.0	10.5	2.0	0.4	20.0	26
	—	—	—	—	—	—	—	—
Podite, width (μm)	11.0	5.0	8.6	9.0	1.7	0.3	20.4	26
	8.0	3.0	5.6	6.0	1.1	0.2	20.4	26
Cell apex to proximal end of left ciliary field, distance (μm)	41.0	6.0	17.5	16.0	7.5	1.5	42.7	26
	14.0	3.0	8.9	9.5	2.9	0.6	32.7	26
Cell apex to distal end of left ciliary field, distance (μm)	77.0	24.0	63.9	67.0	11.5	2.3	18.0	26
	—	—	—	—	—	—	—	—
Left field, length (μm)	—	—	—	—	—	—	—	—
	35.0	17.0	25.2	24.5	5.0	1.0	19.9	26
Circumoral arch, length (μm)	—	—	—	—	—	—	—	—
	13.0	6.0	8.1	8.0	1.6	0.3	19.5	26
Circumoral arch, width (μm)	—	—	—	—	—	—	—	—
	7.0	3.0	4.7	4.5	1.1	0.2	23.2	26
Cell apex to proximal end of preoral kinety, distance (μm)	37.0	22.0	30.4	31.0	4.8	0.9	15.8	26
	18.0	11.0	13.9	14.0	1.8	0.3	12.6	26
Cell apex to proximal end of circumoral kineties, distance (μm)	38.0	20.0	29.9	31.0	5.2	1.0	17.6	26
	17.0	10.0	13.0	13.0	1.6	0.3	12.6	26
Cell apex to distal end of circumoral kineties, distance (μm)	58.0	34.0	48.6	50.5	7.0	1.4	14.5	26

For Review Only

	23.0	16.0	19.1	19.0	1.8	0.4	9.5	26
Cell apex to proximal end of kinetofragments, distance (µm)	174.0	77.0	117.4	119.5	22.8	4.5	19.4	26
	48.0	28.0	37.7	37.0	4.5	0.9	11.8	26
Cell apex to distal end of kinetofragments, distance (µm)	206.0	92.0	136.2	134.5	27.0	5.3	19.8	26
	—	—	—	—	—	—	—	—
Kinetofragments, length (µm)	—	—	—	—	—	—	—	—
	15.0	6.0	9.6	9.0	2.2	0.4	23.4	26
Cell apex to tip of podite, distance (µm)	—	—	—	—	—	—	—	—
	60.0	39.0	47.1	46.0	5.3	1.0	11.2	26
Cell apex to proximal end of cytopharynx, distance (µm)	44.0	24.0	35.1	36.0	5.7	1.1	16.2	26
	—	—	—	—	—	—	—	—
Cell apex to posterior curvature of cytopharynx, distance (µm)	—	—	—	—	—	—	—	—
	34.0	25.0	29.1	28.0	2.2	0.4	7.5	26
Preoral kineties, number	1.0	1.0	1.0	1.0	0.0	0.0	0.0	26
	1.0	1.0	1.0	1.0	0.0	0.0	0.0	26
Circumoral kineties, number	2.0	2.0	2.0	2.0	0.0	0.0	0.0	26
	2.0	2.0	2.0	2.0	0.0	0.0	0.0	26
Infundibular kineties, number	—	—	—	—	—	—	—	—
	13.0	9.0	10.8	11.0	1.2	0.2	11.1	26
Somatic kineties, number	79.0	49.0	66.0	66.0	8.2	1.6	12.4	26
	61.0	45.0	51.5	51.0	3.8	0.7	7.3	26
Right field kineties, number	69.0	37.0	56.0	57.0	8.0	1.6	14.2	26
	58.0	41.0	48.0	47.5	3.7	0.7	7.8	26
Left field kineties, number	13.0	7.0	10.0	10.0	2.0	0.4	19.6	26
	4.0	3.0	3.5	3.5	0.5	0.1	14.6	26
Kinetofragments, number	4.0	4.0	4.0	4.0	0.0	0.0	0.0	26
	4.0	4.0	4.0	4.0	0.0	0.0	0.0	26
Fibrous bundles of non-ciliated surface, number	16.0	11.0	14.5	15.0	1.1	0.2	7.3	26
	—	—	—	—	—	—	—	—
Basal bodies in equatorial fragment, number	28	5	15	15.2	6.7	1.3	43.7	25

For Review Only

Abbreviations: CV, coefficient of variation in %; Max, maximum; Mean, arithmetic mean; Min, minimum; *n*, number of specimens examined; SD, standard deviation; SE, standard error.

For Review Only

Table 2. Accession numbers, lengths and G + C contents of sequences provided in present work.

Species		*K. paracetarius*	*P. ovata*
SSU rDNA	Accession number	MN830168	MN830169
	Length	1677 bp	1552 bp
	GC content	43.71%	44.91%
ITS1-5.8S-ITS2	Accession number	MN830164	MN830165
	Length	421bp	398bp
	GC content	41.81%	41.96%
LSU rDNA	Accession number	MN830170	MN830171
	Length	1739bp	1772bp
	GC content	44.85%	44.70%

For Review Only

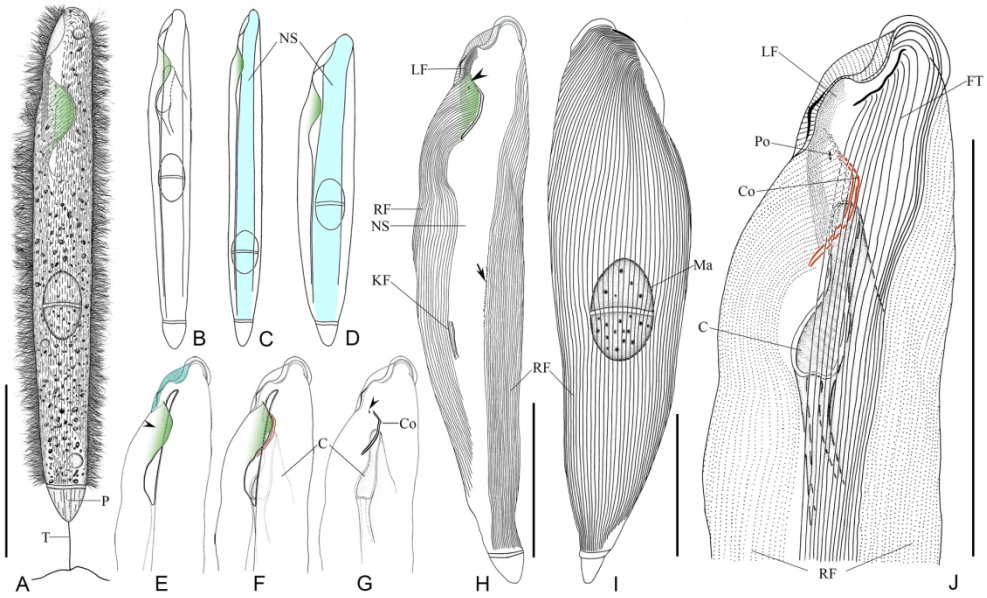

Figure 1, Drawing of n. sp.

169x105mm (300 x 300 DPI)

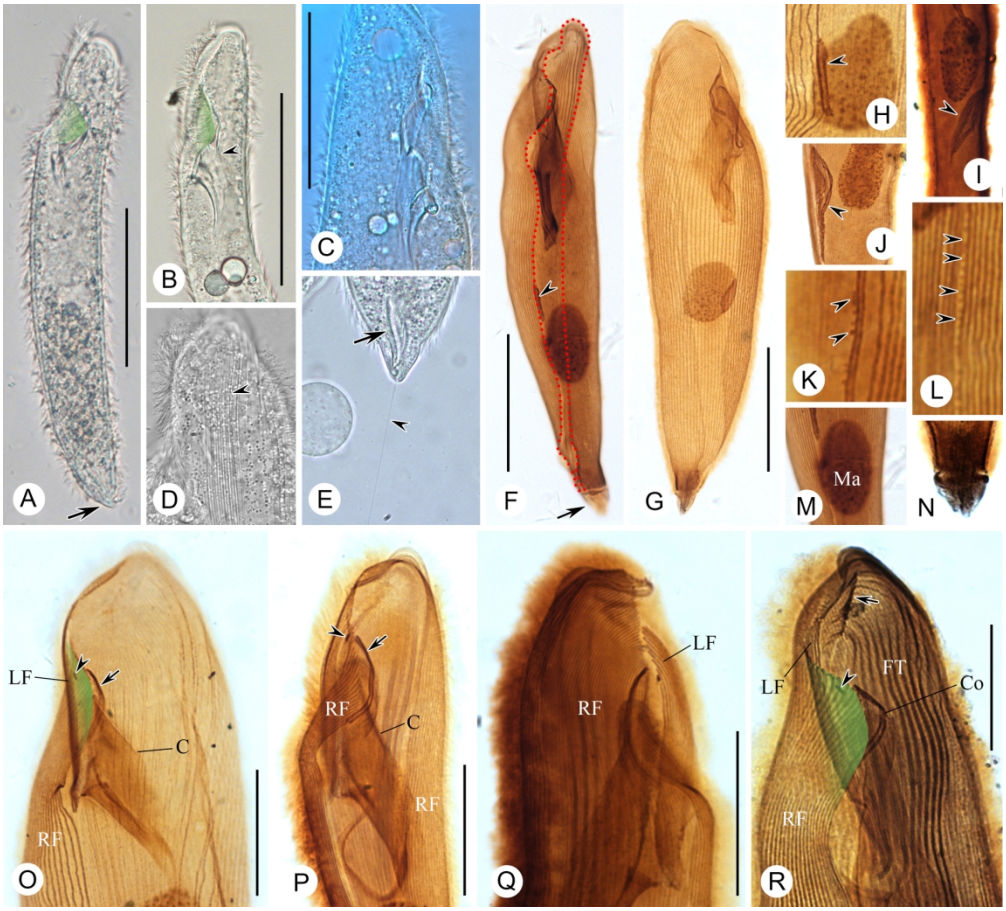

Figure 2, Pictures of n. sp.

170x153mm (300 x 300 DPI)

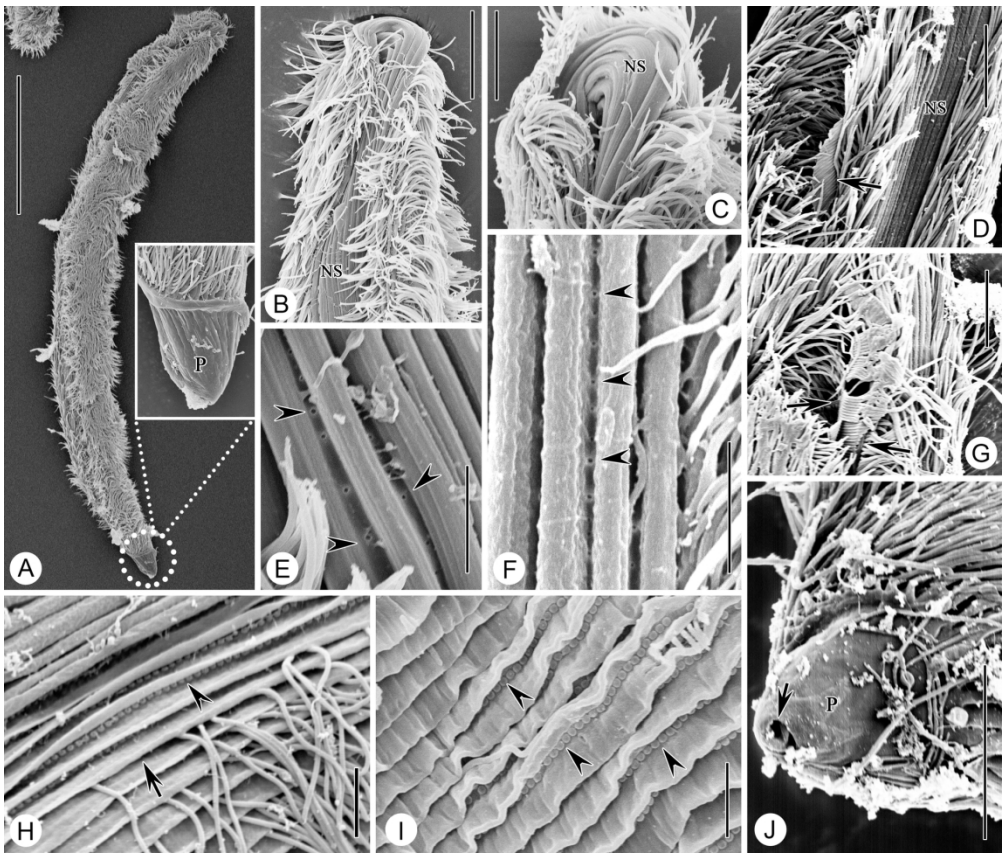

Figure 3, SEM

169x143mm (300 x 300 DPI)

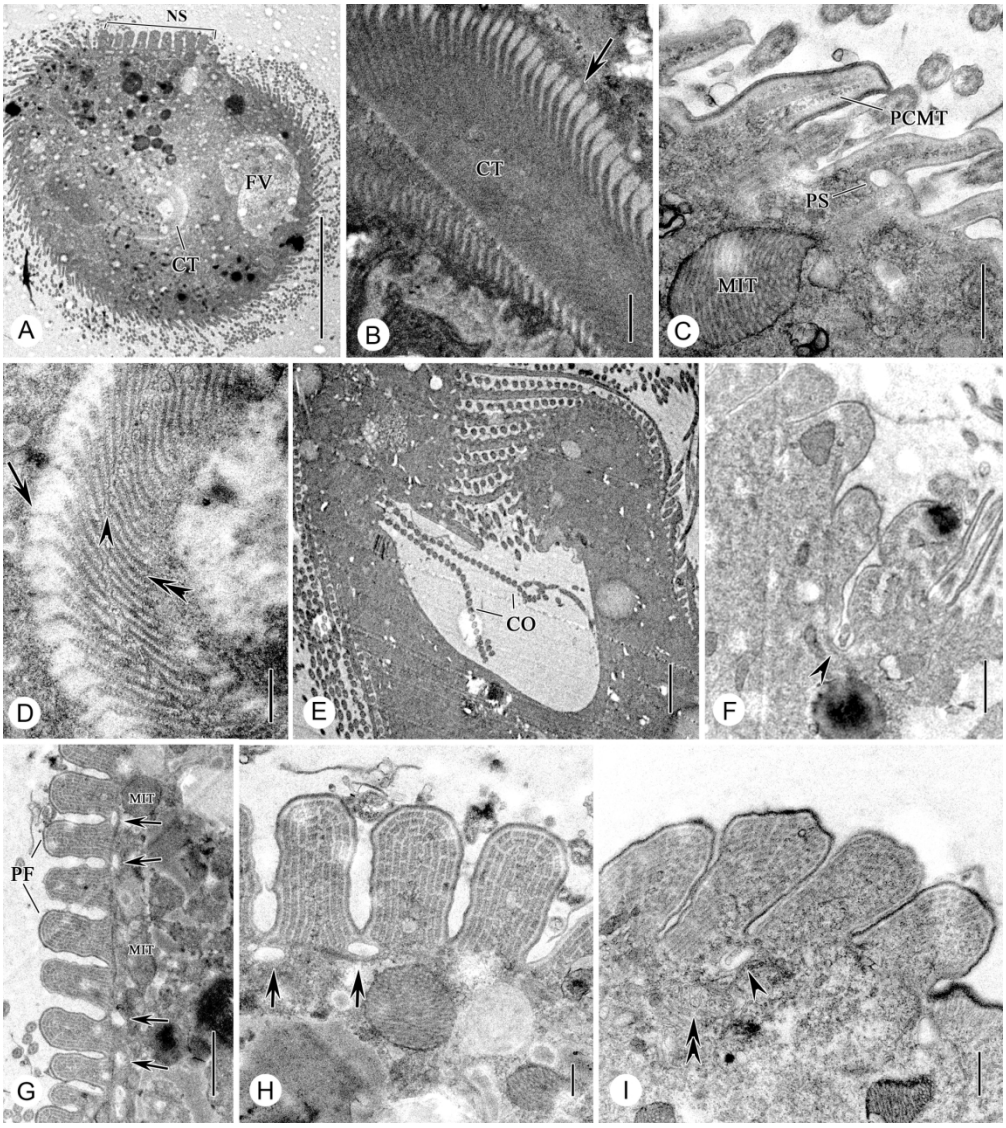

Figure 4, TEM

170x190mm (300 x 300 DPI)

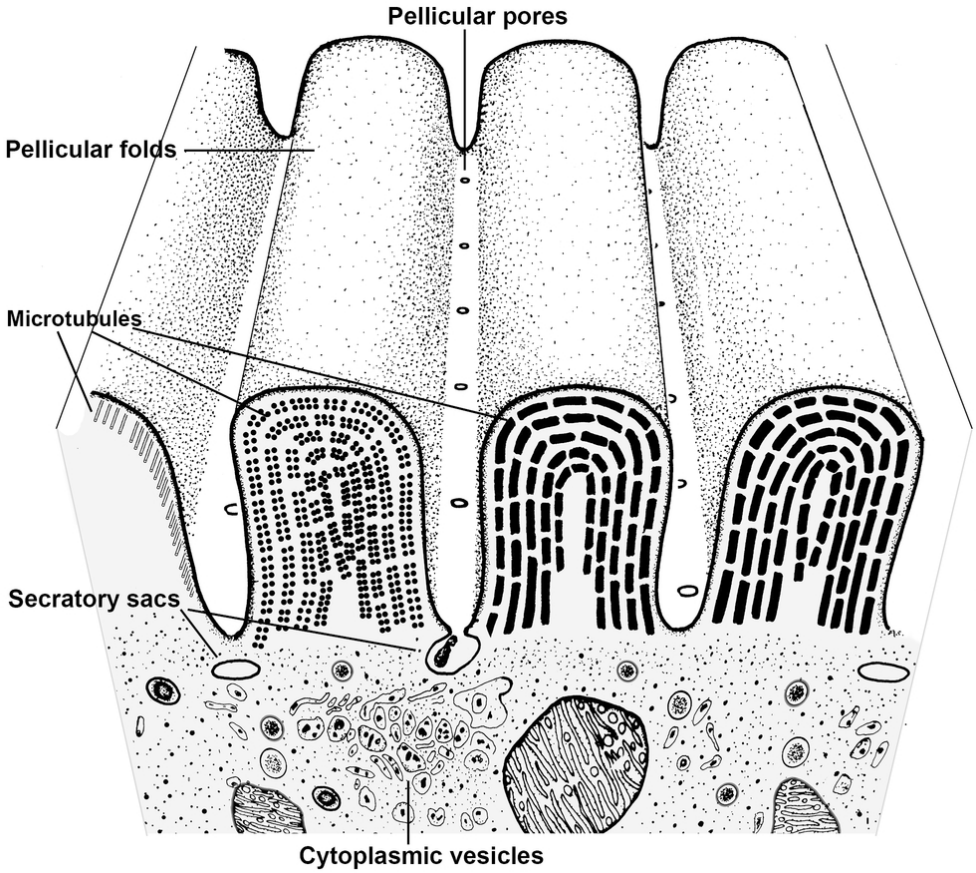

Figure 5, TEM drawing

85x76mm (300 x 300 DPI)

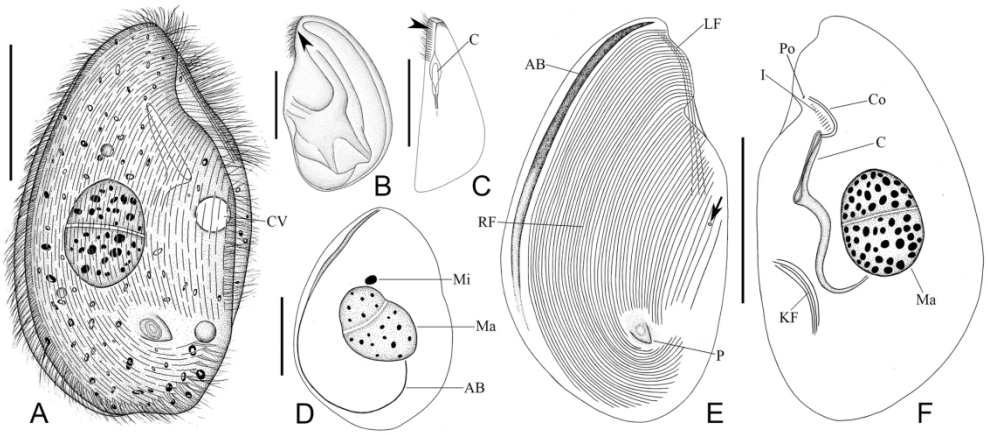

Figure 6, Drawing of P. ovata

170x76mm (300 x 300 DPI)

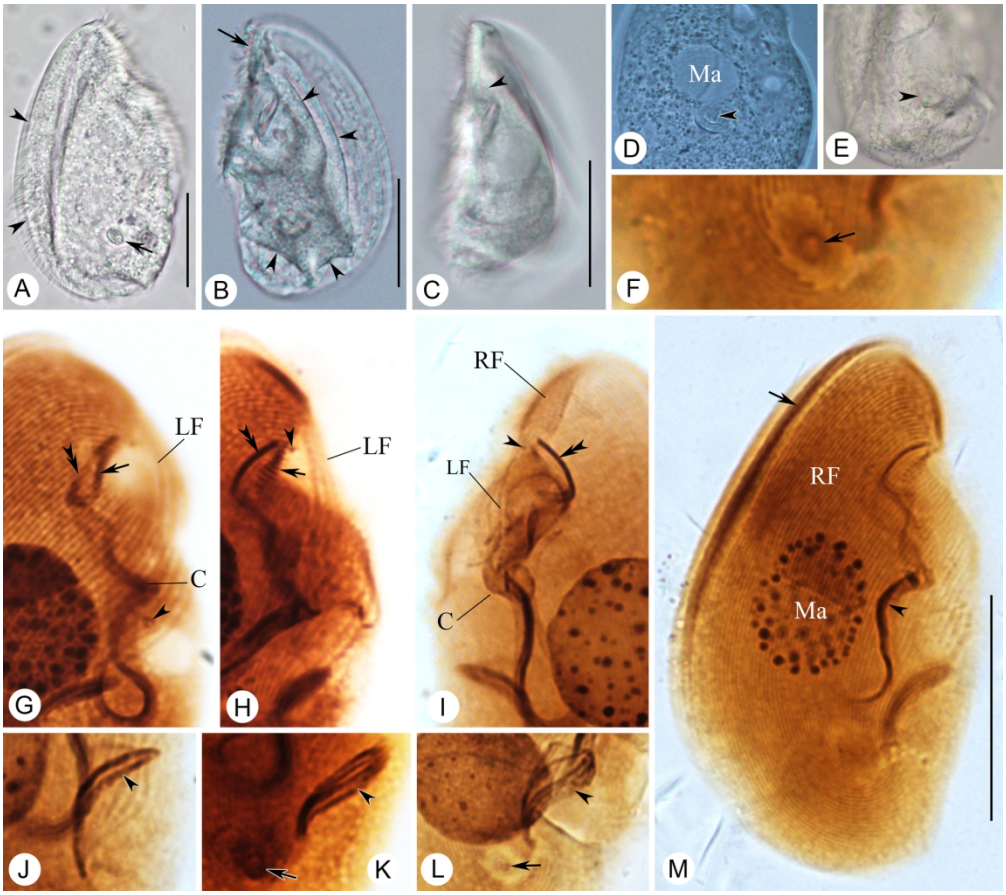

Figure 7

169x150mm (300 x 300 DPI)

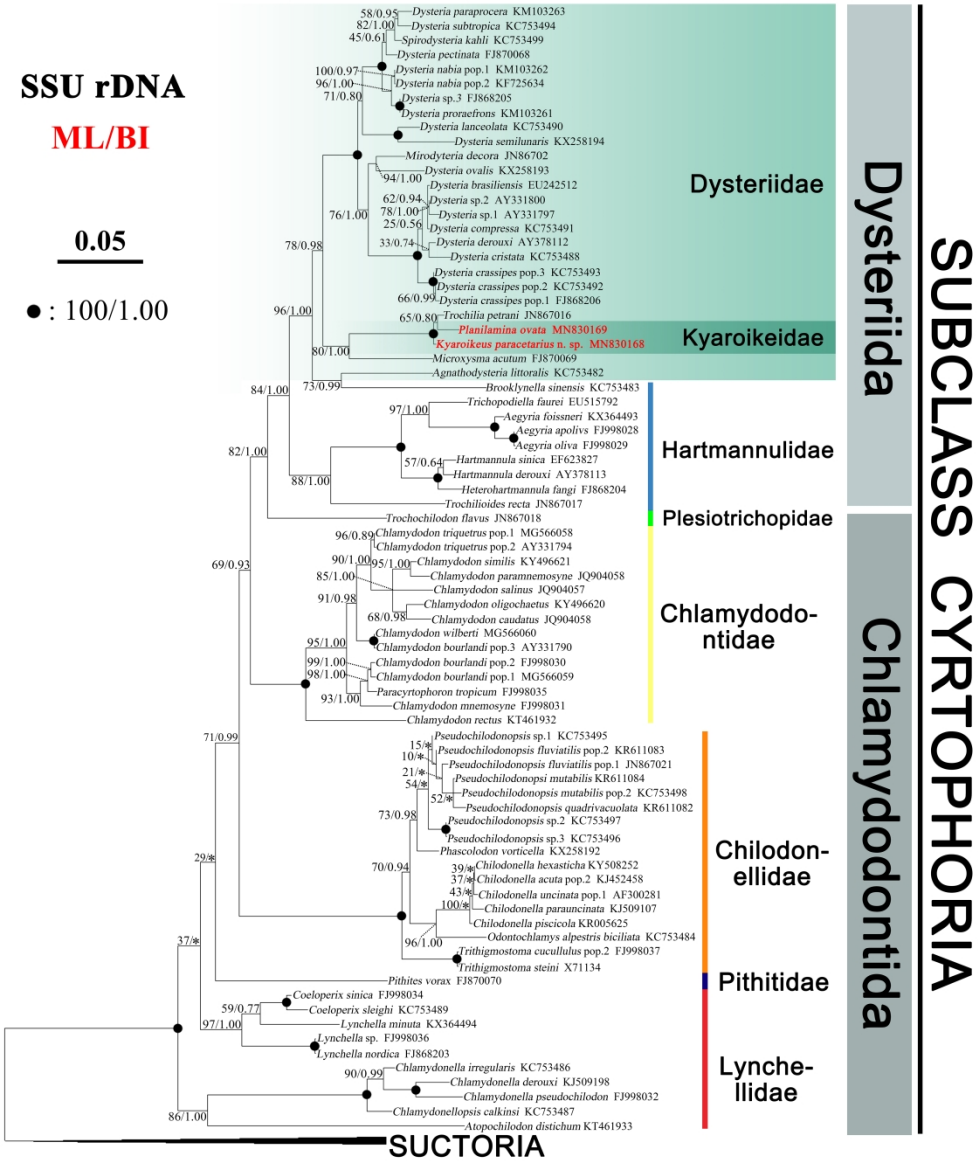

Figure 8, SSU rDNA tree

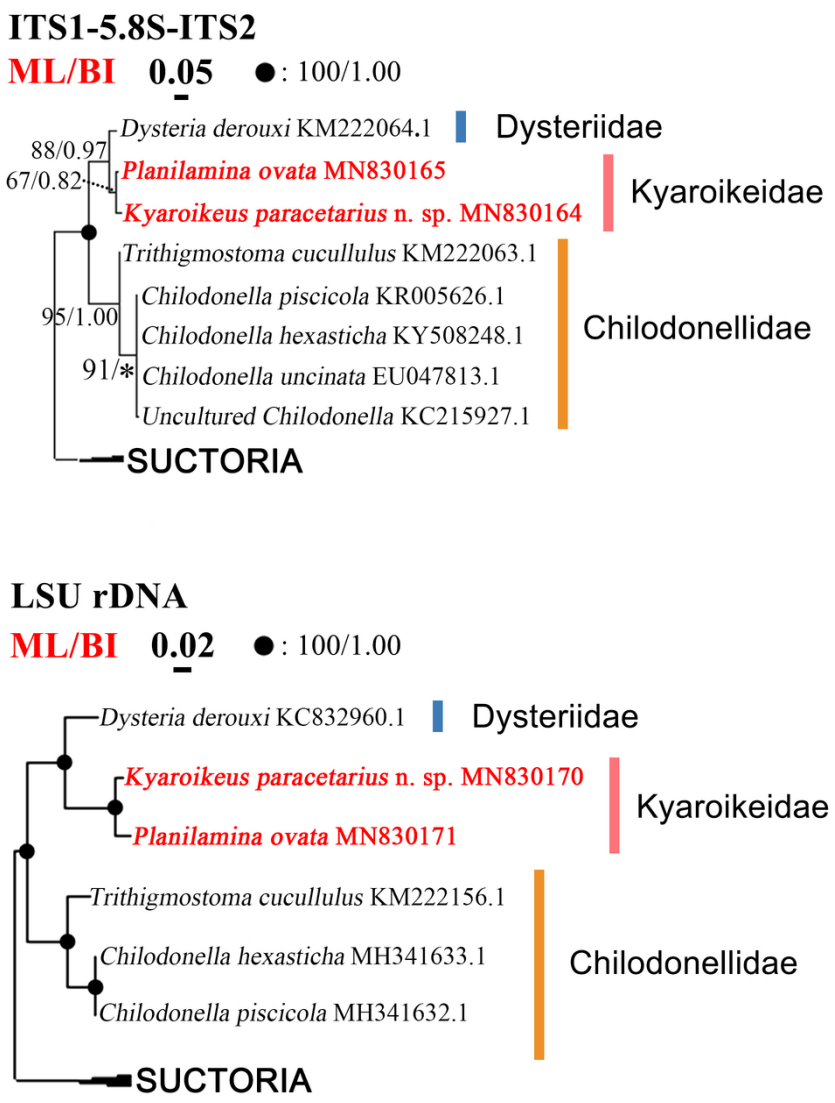

Figure 9, LSU, ITS tree

85x115mm (300 x 300 DPI)

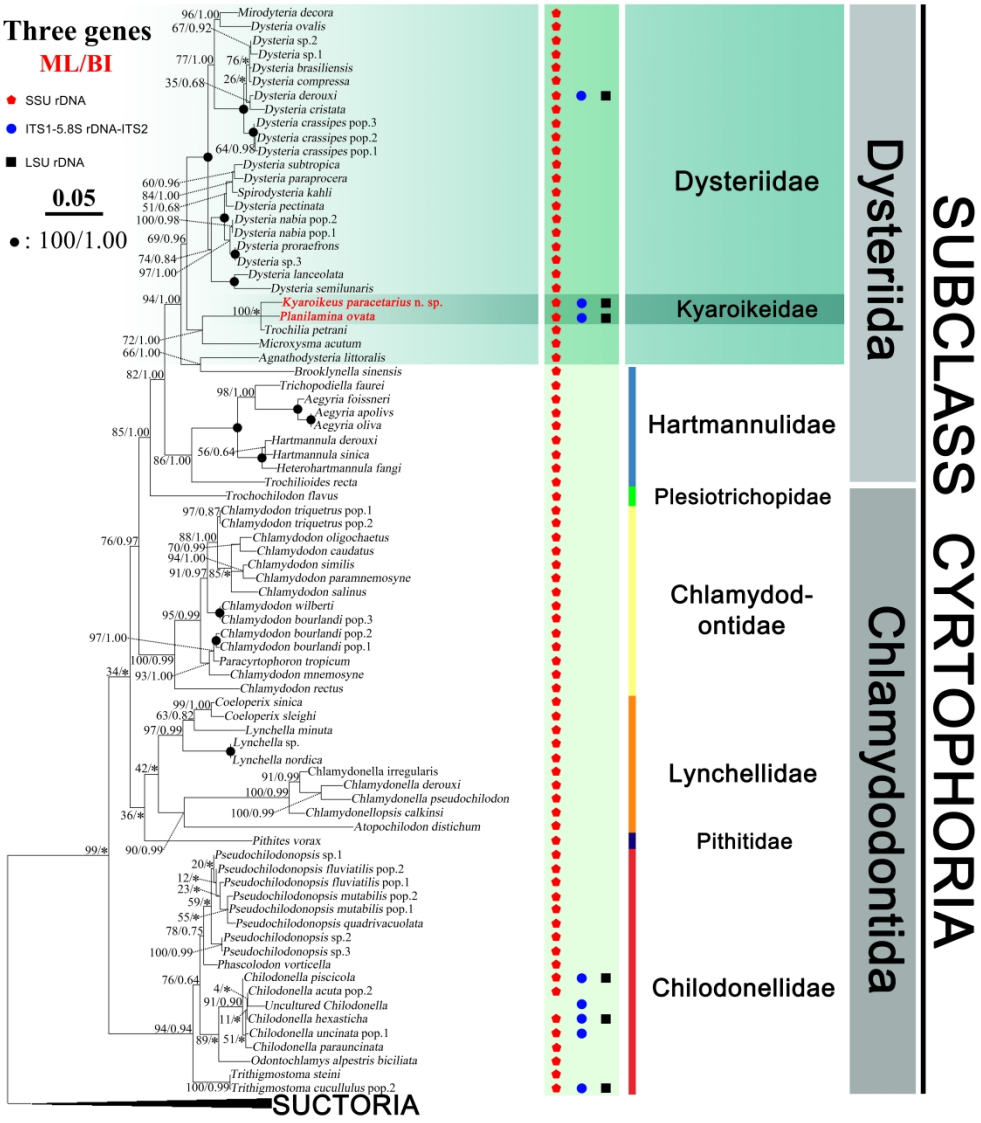

Figure 10, Three genes tree